

# Fast processes in liquid metal foams investigated by high-speed synchrotron X-ray micro-radioscopy

F. García-Moreno

*Institute for Materials Science and Technology,  
Technische Universität Berlin, Germany*

A. Rack, L. Helfen, and T. Baumbach

*Institute for Synchrotron Radiation – ANKA,  
Forschungszentrum Karlsruhe, Germany*

S. Zabler, N. Babcsán, and J. Banhart

*Department of Engineering Materials,  
Helmholtz Centre Berlin (Hahn-Meitner-Institut), Germany*

T. Martin, C. Ponchut, and M. Di Michiel

*European Synchrotron Radiation Facility, Grenoble, France*

## Abstract

Rupture of an individual film in an evolving liquid metal foam is investigated by means of high-speed X-ray radioscopy using white synchrotron radiation. At a frame rate of 5000 fps the rupture event is spread over 3 to 4 images. The images show that the remnants of the rupturing film are pulled into the surrounding plateau borders in  $600 \pm 100 \mu\text{s}$  which conforms well with a liquid movement governed by inertia and not by viscosity. Within one order of magnitude the viscosity of the liquid involved must be similar to the viscosity of pure liquid aluminium.

Many manufacturing processes involve fast movements inside closed containers or flow of opaque liquids such as metallic melts. In many cases knowledge about such processes is necessary to understand functionalities or mechanisms, but a direct visual insight into the system is impossible. Radioscopy with penetrating rays can help to overcome such problems. X-ray radioscopy using X-ray tubes has been used to study such phenomena, e.g. to visualise oxide films during solidification of aluminium alloys [1], growth of hydrogen pores in aluminium castings [2, 3], or convective flow in liquid metals [4]. The flux of conventional X-ray sources limits both the accessible frame rates to a few frames per second (fps) and spatial resolutions to some  $10\text{ }\mu\text{m}$ . Therefore, synchrotron radiation has been applied to study processes in higher spatial and temporal resolution. Recent examples include the growth of dendrites in Al-Ni alloys [5], coarsening of two-phase semisolid alloys [6], water evolution in operating fuel cells [7], or fuel injection into a running engine [8].

An ubiquitous phenomenon in metal foams is coalescence: thermal or mechanical instabilities lead to the rupture of a film separating two adjacent bubbles and the subsequent merger of these. Knowing the dynamics of such rupture events is important since they reflect the properties of the constitutive liquid. It has been estimated that such ruptures take place on the time scale of some ms or even faster [9]. X-ray radioscopy has been shown to be a valuable tool to investigate the details of internal bubble creation and rearrangement in metal foams at high resolutions ( $\approx 10\text{ }\mu\text{m}$ ) and moderate rates ( $\leq 18\text{ fps}$ ) [9, 10]. To image rupture phenomena, a considerable increase in frame acquisition rate is required. In this paper we present an investigation of liquid metallic foams by means of high-speed radioscopy and we capture 5000 images per second to reveal the details of pore coalescence during growth of Al-6%Si-4%Cu (wt.%) alloy foam. We shall first describe the imaging technique and then present the results of an experiment on metallic foam.

The foaming furnace setup is shown in Fig. 1. It consists of a ceramic heating plate placed inside a gas-tight aluminium cylinder (wall thickness: 0.5 mm) that allows for pressure variations. The furnace is equipped with connections for heating current, thermocouples and gas in- and outlets and has already been described in more detail elsewhere [11]. For foaming, the furnace was loaded with a  $10 \times 5 \times 4\text{ mm}^3$  large piece of foamable precursor, the 5 mm-side oriented in the beam direction. The precursor was manufactured by powder pressing [10] and contained the aluminium alloy and 0.5 wt.% of uniformly dispersed  $\text{TiH}_2$  particles acting as a blowing agent. The container was pressurised with 5 bar argon gas, after which the sample

was heated to  $T = 600^\circ\text{C}$  within 20 s. After melting, the gas contained in the blowing agent nucleated in the sample leading to a small volume expansion of about 5 to 10%. In a next step, the vessel was depressurized to ambient pressure in about 5 s which caused rapid growth of the foam and triggered additional cell wall ruptures [12]. Foaming could also be carried out at constant ambient pressure, but under such conditions too few rupture events would occur in the short time window available for radioscopy viewing ( $\approx 1$  s), the limit given by the available storage capacity of the camera memory and the image acquisition rate used.

Imaging experiments were carried out at beamline ID19 of the European Synchrotron ESRF (Grenoble, France). A quasi-white spectrum of ID19's wiggler (gap 40 mm) was used in order to have a flux of  $\approx 10^{15}$  Ph/mm<sup>2</sup>/s suitable for our fast imaging application. The beam was filtered by 1.5 mm of aluminium (including the two pressure vessel walls).

Different detector concepts for high resolution synchrotron imaging are known [13, 14]. The classical setup is based on a scintillating screen: its luminescence image is optically coupled via lenses onto a digital camera chip, typically a CCD with a high dynamic range [13]. Such a detector system works with high efficiency at resolutions of a few  $\mu\text{m}$ . Upon increasing resolution the efficiency of indirect detection decreases dramatically due to the small thickness required for the scintillating screens (down to 5  $\mu\text{m}$  for sub- $\mu\text{m}$  resolution) [15]. The speed of such a detector system is limited by the readout rate of the CCD, typically in the range of several fps up to several hundred fps, depending on the number of pixels, dynamic range, readout design of the CCD etc. [16].

Higher frame rates can easily be reached by applying direct X-ray detectors such as, e.g. Medipix2 [17]. These direct detectors can be described as CMOS chips with a photodiode coupled to each pixel. For selected diffraction applications even standard CMOS chips designed for detecting visible light have been applied to fast direct X-ray detection [18]. Their maximum resolution is limited to the intrinsic pixel size of the chips. The life time depends on energy and flux of the radiation used.

As we aimed at using the highly intense white beam of a wiggler source we compromised by using a CMOS camera for visible light detection in an indirect detection setup, see Fig. 1. For the scintillating screen we chose a 300  $\mu\text{m}$  thick YAG:Ce single crystal. YAG:Ce is one of the few known materials that are commercially available and have already been applied in synchrotron imaging with a high heat load [19]. In particular, the material does not show

a decreasing light yield with increasing temperature [20]. Directly behind the scintillator a mirror is placed, resulting in a folded beam path of the visible light. The luminescence image of the YAG:Ce screen is projected with a low-magnifying, long working-distance objective onto a digital camera situated outside of the synchrotron beam. The result is a design where no detector parts that could be damaged by ionizing radiation are facing the high flux of high energy X-rays. As fast camera we chose a PCO.1200 hs (1280×1024 pixels, 10 bit dynamic range – 60 dB, 12 μm pixel size, 25 % peak efficiency at 520 nm, up to 1 GB/s recording speed). This system allows us to image our foam with 1357 fps at VGA resolution (9 μm effective pixel size). In order to reach the required 5000 fps (200 μs exposure time) we restricted the region-of-interest to 1280×128 pixels.

In Fig. 2 we can observe the rupture process of an individual film within a AlSi6Cu4 foam in high time resolution [? ]. In the first image the encircled vertex of three films is still intact. 200 μs later in the second image the film extending to the lower right is already interrupted and the liquid metal is being pulled to the upper left as indicated by the arrow. In the third and fourth images this liquid rearrangement continues. After 800 μs the movement has come to an end and the last two images show little difference. The diameter of the bubbles in question is in the range of 3 mm.

Radioscopy naturally does not reveal the true position of all the material and therefore we cannot specify how the rupture event initiated and to where exactly the metal in the ruptured features has been redistributed. Assuming the simple picture of a line-shaped distortion within a square film of an ideal liquid, dimensions  $b \times b$  and uniform thickness  $c$ , the rupture time  $T_r$  of such a film consisting of a liquid with density  $\rho$  and surface tension  $\sigma$  can be estimated (Ref. 9 with additional factor 2 to account for the two interfaces of the film):

$$T_r = \frac{b}{2} \sqrt{\frac{c\rho}{2\sigma}} \approx 500 \mu s,$$

using  $b=3$  mm,  $c=80$  μm,  $\rho=2380$  kg/m<sup>3</sup>,  $\sigma=0.87$  N/m [9]. The latter values are for pure aluminium, but the values for the alloy should be very similar. From our experiment we estimate  $T_r \approx 600 \pm 100$  μs which is in a reasonable agreement with this value but due to the simplicity of the model and the crude estimates of the values used in the equation this should not be over-interpreted. Analysis of further rupture phenomena yielded rupture times between 400 and 1000 μs.

In this model the surface force accelerating the melt is simply  $F_s = 2\sigma b \approx 5 \text{ mN}$ . The average viscous force  $F_v$  due to the viscosity of the liquid  $\eta$ , acting against  $F_s$ , can be estimated by applying a textbook equation based on laminar flow in the film:  $F_v = \eta v \frac{b^2}{c}$ , where  $v$  is the average velocity. Pure aluminium has  $\eta \approx 1.5 \text{ mPas}$ , and hence  $F_v \approx 0.36 \text{ mN} \approx \frac{1}{14} F_s$ . In this case the liquid movement is largely dominated by inertia. This shows that individual films break in a time suggesting that the effective viscosity is that of the pure liquid within one order of magnitude.

In the literature a foam-stabilizing mechanism via a dramatically enhanced viscosity has been proposed which is caused by the formation of a filigree network of oxides forming a gel. It is found that an apparent viscosity of  $400 \text{ mPas}$  explains the observed stability of foam columns [21]. With such a high value for  $\eta$  we would get  $F_v \approx 20 F_s$ , and viscous damping would lead to measurably higher values for  $T_r$ . A network of oxide fragments – clearly discernible in microscopic images [22] – might give rise to a high viscosity in an undistorted state and block liquid flow out of the films. After rupture, however, this network seems to have broken up. The viscosity of the liquid in the film appears to depend highly on the history of the melt and the forces acting on it.

In conclusion, using white synchrotron X-ray radiation, a suitable fluorescent screen and a fast CMOS camera, X-ray image sequences with up to  $5000 \text{ fps}$  can be acquired. The temporal evolution of the rupture of an individual metal film within a metallic foam was observed. The observed rupture time of about  $600 \pm 100 \mu\text{s}$  is in agreement with a simple model that assumes inertia-limited film rupture and expresses the fact that the liquid in rupturing films is very fluid and behaves like a conventional melt.

We acknowledge funding by the European Space Agency via MAP projects AO99-075 and XRMON.

- 
- [1] S. Fox and J. Campbell, *Scripta Mater.* **43**, 881 (2000).
- [2] P. Lee and J. Hunt, *Acta Mater.* **45**, 4135 (1997).
- [3] R. Atwood, S. Sridhar, W. Zhang, and P. Lee, *Acta Mater.* **48**, 405 (2000).
- [4] J. Koster, T. Seidel, and R. Derebail, *J. Fluid Mech.* **343**, 29 (1997).
- [5] A. MacPhee, M. Tate, C. Powell, Y. Yue, M. Renzi, A. Ercan, S. Narayanan, E. Fontes, J. Walther, J. Schaller, et al., *Science* **295**, 1261 (2002).
- [6] S. Zabler, A. Rueda, A. Rack, H. Riesemeier, P. Zaslansky, I. Manke, F. García-Moreno, and J. Banhart, *Acta Mater.* **55**, 5045 (2007).
- [7] I. Manke, C. Hartnig, M. Grünerbel, W. Lehnert, N. Kardjilov, A. Haibel, A. Hilger, and J. Banhart, *Appl. Phys. Lett.* **90**, 174105 (2007).
- [8] N. Mangelinck-Noël, H. Nguyen-Thi, G. Reinhart, T. Schenk, V. Cristiglio, M.-D. Doupouy, J. Gastaldi, B. Billia, J. Härtwig, and J. Baruchel, *J. Phys. D: Appl. Phys.* **38**, A28 (2005).
- [9] H. Stanzick, M. Wichmann, J. Weise, L. Helfen, T. Baumbach, and J. Banhart, *Adv. Eng. Mater.* **4**, 814 (2002).
- [10] J. Banhart, H. Stanzick, L. Helfen, and T. Baumbach, *Appl. Phys. Lett.* **78**, 1152 (2001).
- [11] F. García-Moreno, N. Babcsán, and J. Banhart, *Coll. Surf. A* **263**, 290 (2005).
- [12] F. García-Moreno and J. Banhart, *Coll. Surf. A* **309**, 264 (2007).
- [13] U. Bonse and F. Busch, *Prog. Biophys. Molec. Biol.* **65**, 133 (1996).
- [14] H. Graafsma and T. Martin, in *Advanced Tomographic Methods in Materials Research and Engineering*, edited by J. Banhart (Oxford University Press, 2008), p. 277.
- [15] A. Koch, C. Raven, P. Spanne, and A. Snigirev, *J. Opt. Soc. Am.* **15**, 1940 (1998).
- [16] S. Gruner, M. Tate, and E. F. Eikenberry, *Rev. Sci. Instr.* **73**, 2815 (1998).
- [17] G. Mettivier, M. Montesi, A. Sebastiano, and P. Russo, *IEEE Trans. Nucl. Sci.* **53**, 2931 (2006).
- [18] L. Marschand, X. Jiao, M. Sprung, B. Tieman, L. B. Lurio, and A. R. Sandy, in *Proc. 5th International Conference on Synchrotron Radiation in Materials Science (SRMS-5)* (2007).
- [19] M. Di Michiel, J. M. Merino, D. Fernandez-Carreiras, T. Buslaps, V. Honkimäki, P. Falus, T. Martins, and O. Svensson, *Rev. Sci. Instrum.* **76**, 043702 (2005).
- [20] E. Zych, C. Brecher, and J. Glodo, *J. Phys.: Condens. Matter* **12**, 1947 (2000).

[21] V. Gergely and T. W. Clyne, *Acta Mater.* **52**, 3047 (2004).

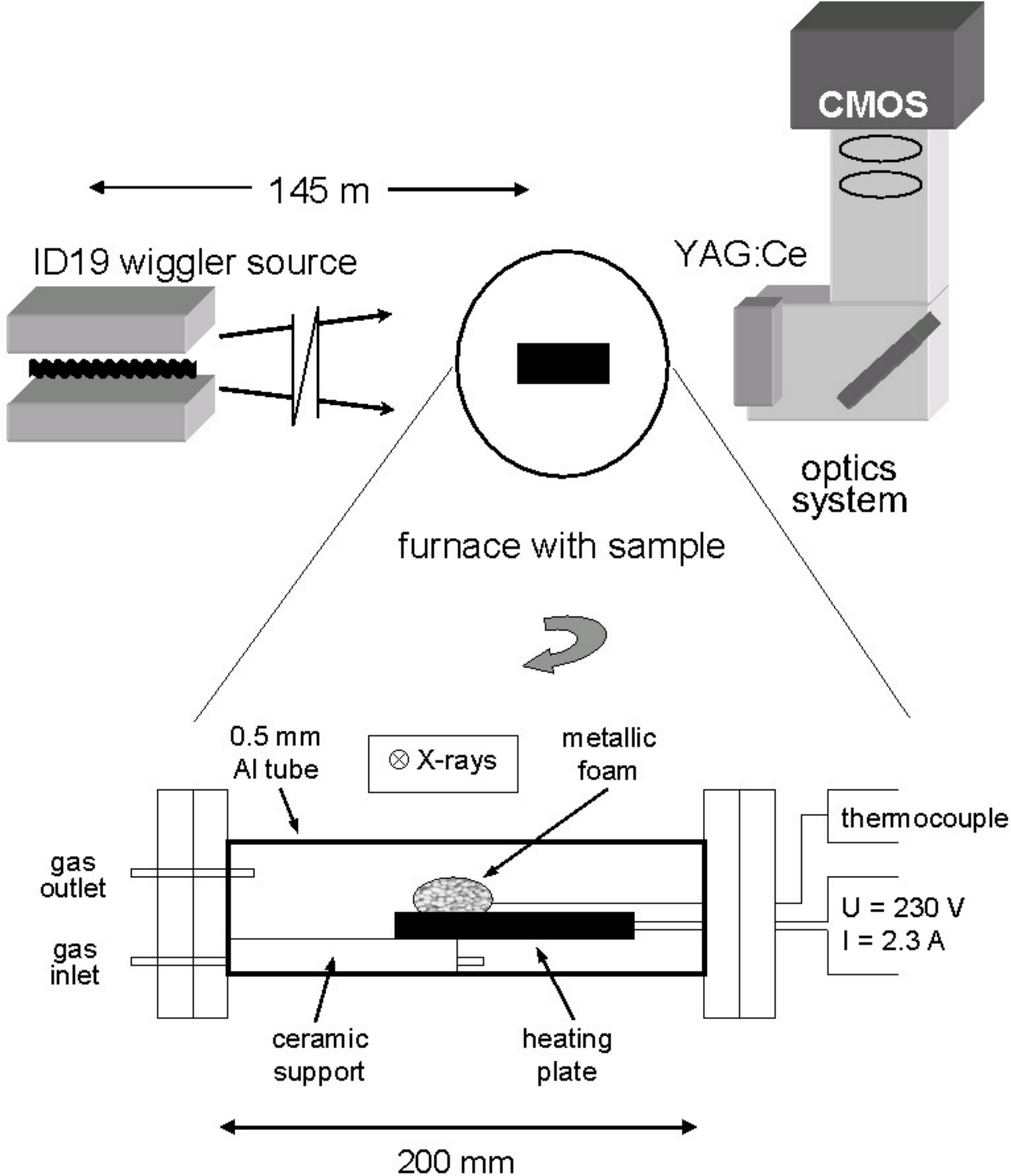
[22] C. Körner, M. Arnold, and R. F. Singer, *Mat. Sci. Eng. A* **396**, 28 (2005).

[] See EPAPS Document No. XXX for the full image sequence. This document can be reached through a direct link in the online articles HTML reference section or via the EPAPS homepage (<http://www.aip.org/pubservs/epaps.html>).

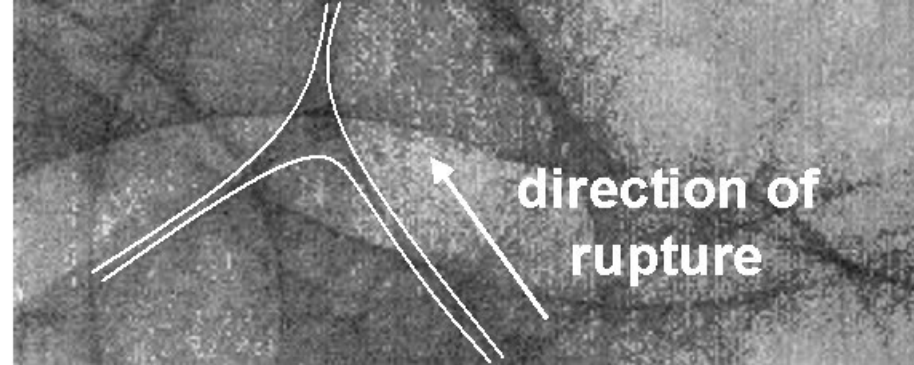
FIG. 1: Sketch of the fast imaging setup used at the beamline ID19 of the ESRF (top), furnace used for in-situ radioscopy experiment viewed in the direction of radiation (bottom).

FIG. 2: Radiographs of a metal foam featuring a rupturing film. Images are  $200\text{ }\mu\text{s}$  apart. First image is reproduced twice to show the position of the rupturing film.





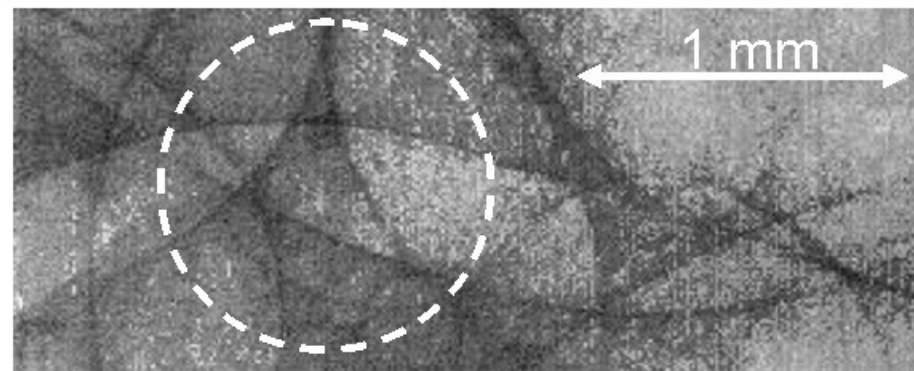
1



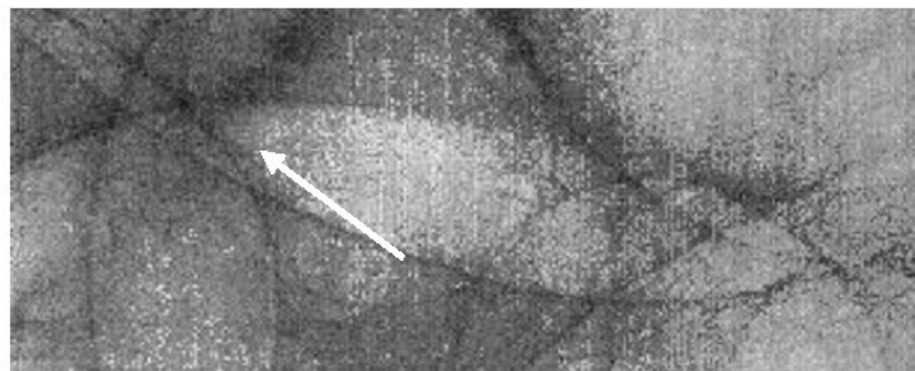
3



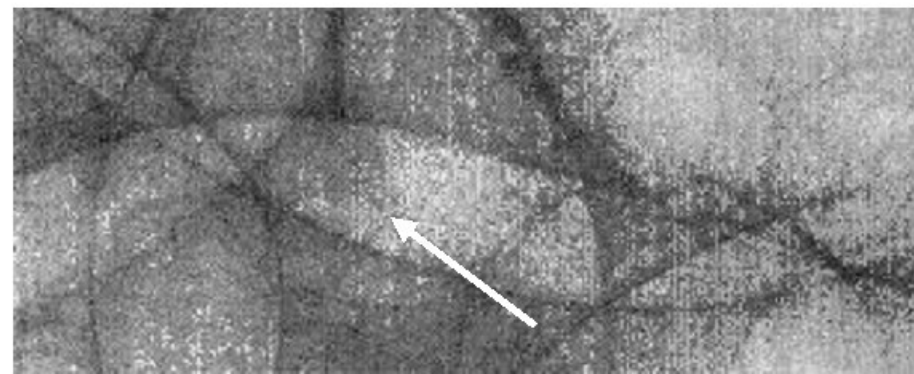
1



4



2



5

